Microstructure Design and Heat Treatment Selection for Casting Alloys Using the Quality Index

C.H. Cáceres

(Submitted 12 December 1999; in revised form 3 January 2000)

The ductility of casting alloys is usually low and it is thus important to simultaneously assess the effect of changes to the microstructure and heat treatment on both ductility and strength of the material. The use for this purpose of the quality index charts* is common in the casting industry with regard to the Al-Si-Mg casting alloys A356 and A357.

An analytical method of generating quality index charts for any alloy system is presented. Applications of the method are illustrated with case studies involving Al-Si-Mg, Mg-Al-Zn, and Al-Si-Cu-Mg casting alloys. The analytically determined charts indicate the limits to microstructural improvement available for each material. The possibility of using the charts to optimize the relation between mechanical performance, chemical composition, solidification conditions, and temper is discussed.

Keywords casting, Al-Si-Mg alloys, Mg-Al-Zn alloys, Al-Cu-Si alloys, strength, ductility, heat treatment

1. Introduction

The ductility of casting alloys is usually low, and changes to the casting process as well as changes in the chemical composition and/or heat treatment aimed at improving the strength or other properties can render the material too brittle for structural applications. It is thus important to simultaneously assess the effect of any changes to the microstructure on the ductility and strength of the material. This analysis proposes the use of strength-ductility diagrams known as quality index charts,[1] an example of which is shown in Fig. 1, to select the temper and chemical composition that optimize the mechanical performance of casting alloys.

High tensile strength, *TS,* and high tensile ductility, s_f, are most desirable properties in structural design, and if the chart from Fig. 1 is used to plot the experimentally determined *TS* and s_f values for a particular alloy, the best "quality" material will be located near the upper right corner. Different materials or processing conditions can thus be assessed on the basis of their locus on the chart. This is partly the logic behind the development of the quality index charts, a concept developed in the 1970s by Drouzy *et al.*[1] with reference to alloys A356/A357.

The chart of Fig. 1 has two main axes representing tensile strength and ductility. The dashed lines across the diagram are called iso-*Q* and iso-yield strength lines, respectively, and serve to identify the quality index, *Q,* and the yield strength, *YS,* respectively, of any data point on the chart. In its most straightforward application, the chart allows a comparison of the quality of experimental data from different alloys, or from different batches of samples of the same alloy through the corresponding *Q* values.

C.H. Cáceres, CRC for Alloy and Solidification Technology (CAST), Department of Mining, Minerals and Materials Engineering, The University of Queensland, Brisbane QLD 4072, Australia.

*M. Drouzy, S. Jacob, and M. Richard: *AFS Int. Cast Met. J.,* 1980, vol. 5, pp. 43–50.

In the original charts,[1] the iso-*Q* lines are determined by the following empirical relationship between the tensile strength and the elongation to fracture (%) of the material:

$$Q = TS + d \log (s_f) \quad \text{(Eq 1)}$$

With reference to Fig. 1, the *Q* value is defined as the *y* intercept of Eq 1 at $s_f = 1\%$.

The "iso-yield strength" lines are defined by

$$YS = aTS - b \log (s_f) - c \quad \text{(Eq 2)}$$

where *YS* is the (0.2% offset) yield stress. The parameters *a, b, c,* and *d* are empirically determined constants whose values depend on the alloy system.[1,3]

The concept was introduced with reference to the Al-7% Si-Mg casting alloys A356/357. However, a recent theoretical model has shown that it can be naturally extended to other alloy systems.[2–6]

The theoretical model allows the generation of quality index charts for any given material once the parameters of the deformation curves for different tempers are known. The analytical chart determines the theoretical upper bound to the alloy's ductility based on the onset of necking and indicates how much room for improvement in the microstructure and hence on the mechanical properties is available. Unlike the empirical charts that use alloy A356 as a reference, the analytical charts provide an absolute reference for the studied material.

In what follows, the analytical method used to develop the quality index charts will be briefly outlined. Subsequently, three case studies, involving application of the analytical charts to Al-Si-Mg, Mg-Al-Zn, and Al-Cu-Si casting alloys, will be discussed.

2. Material Parameters and Quality Index

The analytical model[2] leading to the quality index chart is based on the assumption that the deformation curves of the material can be described with a simplified version of the Ramberg-Osgood relationship:

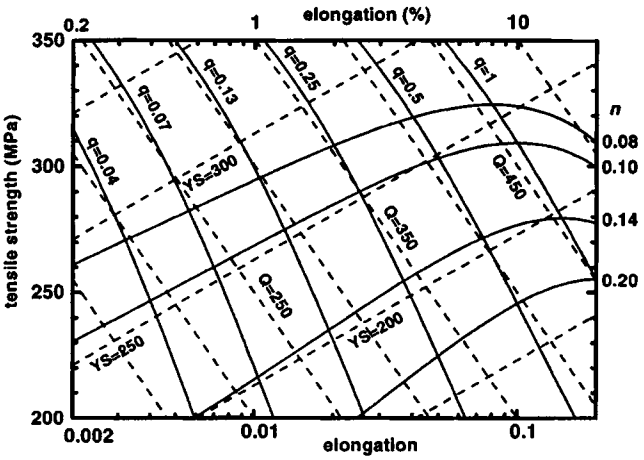

Fig. 1 A quality index chart for alloy A356. The dashed lines are iso-*Q* lines, calculated with Eq 1, and iso-YS lines, calculated with Eq 2.[1] The solid lines are flow curves (calculated with Eq 4 identified by the *n* value) and iso-*q* lines (calculated with Eq 6, identified by the *q* value), respectively, assuming $K = 430$ MPa

$$\sigma = K\varepsilon^n \qquad \text{(Eq 3)}$$

where σ is the true flow stress, K is the alloy strength coefficient, ε is the true plastic strain, and n is the strain hardening exponent. Application of the Considère criterion[7] to Eq 3 shows that necking occurs when $\varepsilon = n$.

The nominal stress-strain curve can be approximated from Eq 3, ignoring the elastic component of the total strain, by

$$P \cong Ks^n e^{-s} \qquad \text{(Eq 4)}$$

where P and s are the engineering values of the stress and the strain. The flow curves (solid lines in Fig. 1, identified by the n value) are generated with Eq 4.

The ductility of the material can be measured with reference to the onset of necking strain by the relative ductility parameter, q, defined as

$$q = \frac{s_f}{n} \qquad \text{(Eq 5)}$$

Solving Eq 5 for n and replacing in Eq 4,

$$P = Ks^{s/q} e^{-s} \qquad \text{(Eq 6)}$$

The iso-q lines in Fig. 1 (solid lines, identified by the q value) were generated with Eq 6. These lines meet the condition of constant relative ductility. The physical meaning of q is such that when $q = 1$ the sample reaches necking, while $q < 1$ values identify progressively less ductile samples. Thus, $q = 0.5$, 0.3, and 0.1 values correspond to samples that fail at 50, 30, and 10% of their necking onset strain, respectively. The correlation between iso-q lines and iso-Q lines shown by Fig. 1 provides a straightforward physical meaning for the quality index in terms of the relative ductility parameter.

A theoretical value for d in Eq 1 can be obtained by differentiating Eq 6 at $q = 1$, which yields[3]

$$d = -\frac{dP}{ds} \cong 0.4K \qquad (q = 1) \qquad \text{(Eq 7)}$$

Substitution of Eqs 4, 5, and 7 into Eq 1 leads to

$$Q = K[(qn)^n e^{-qn} + 0.4 \log (100qn)] \qquad \text{(Eq 8)}$$

The term in square brackets depends very weakly on n, and a convenient approximation for Eq 8 is[8]

$$Q \approx K[1.12 + 0.22 \ln (q)] \qquad \text{(Eq 9)}$$

Notice that K is the only material parameter involved in Eq 6. Thus, if K does not change as the material is aged, the TS-s_f data points lie on a single iso-q line in Fig. 1. (An example is given in the next section, Fig. 3.) In other words, a constant K is a necessary condition for the material to keep its quality constant during the aging process. This conclusion is also evident from Eq 9. A constant Q value when the material is increasingly aged, or, in terms of Eqs 4, 6, and 9, a constant K as n changes with the aging, is the fundamental observation that led to the development of the concept of quality index by Drouzy *et al.*[1] for Al-7%Si-Mg alloys. The analytical lines of Fig. 1 have been calculated for alloy A356, for which K is constant at 430 MPa for all tempers.[2]

Should K vary during the aging process[3] or due to changes in the alloy's chemical composition,[9] both the position (Eq 6) and the slope (Eq 7) of the iso-q lines change. Three possible situations can be anticipated, depending on whether K and Q remain constant as the material is aged. These are as follows:

- constant K and Q values as the material is aged, as in the aluminum alloy A356/A357;
- a constant K value but variable Q, as is found in the Mg-based alloy AZ91; and
- both K and Q change with increasing aging, as in the case of Cu-containing Al alloys.

These three cases will be discussed in the next sections.

3. Application to Al and Mg-Based Alloys

3.1 Case Study 1: K and Q Constant with Aging

With reference to the chart in Fig. 1, a Q value above 400 MPa is considered very good for alloy A356. The Q value does not depend much on the temper or the Mg content, and thus, the quality of the casting is mainly determined by process-related parameters such as the dendrite arm spacing, DAS, the porosity content, Fe-rich intermetallics, dross, and inclusions. Application of the analytical method to generate the quality index chart to this alloy is explained in relation to Fig. 2, where flow curves of the alloy in different tempers are shown. The dashed lines represent fitted functions of the form of Eq 3, with $K = 430$ MPa and n values between 0.2 and 0.08. The solid lines of Fig. 1 were generated using these parameter values in Eqs 4 and 6.

Comparison with experimental data points is shown in Fig. 3 and 4. In Fig. 3, the aging behavior of alloy A356 at two different aging temperatures is illustrated using data from Shivkumar

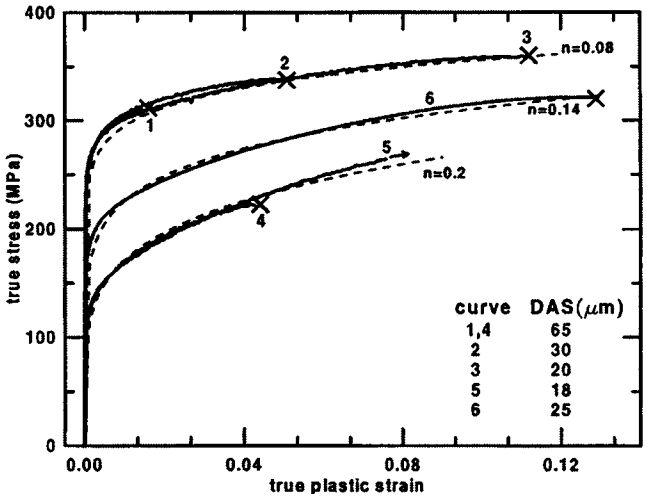

Fig. 2 Flow curves of samples of alloy A356, under different tempers. The dashed lines are functions of the form of Eq 3 with $K = 430$ MPa and given n values

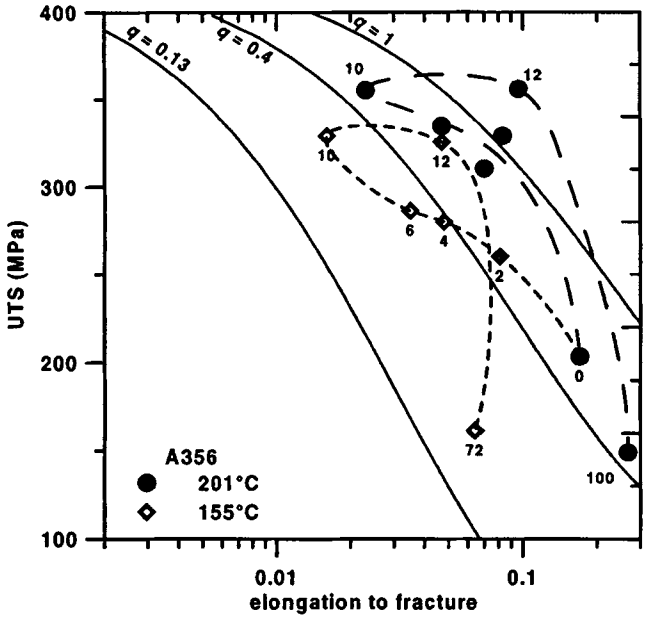

Fig. 3 Strength-ductility behavior of alloy A356 during aging at two different temperatures (data points from Ref 10). The labels indicate the aging time (h). Solid lines calculated with Eq 6

et al.[10] It is seen that the data points follow the trend indicated by the calculated iso-q lines. This is an example of data points moving along a single iso-q line along the entire aging process, including significant overaging.

The influence of the microstructural factors is shown in Fig. 4 using experimental results by Barresi *et al.*[11] Data points representing material with three different Mg and Fe levels, and three different DAS, in T-6 temper are plotted. A number of observations are possible from this chart. First, the material with DAS = 20 μm and lower Fe content fails to the right of the line with $q = 1$, which indicates that the samples failed past the onset

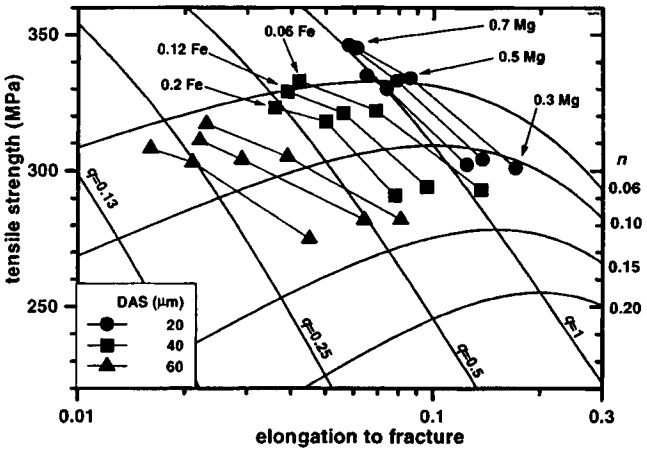

Fig. 4 The effect of the DAS and the Mg and Fe content on the strength and ductility of alloys A356/357.[11] The Mg level changes as indicated for the points with DAS = 20 μm; the level of Fe changes as for the points with DAS = 40 μm

of necking, especially the samples with 0.3%Mg. Increasing the Fe level or the DAS at a given Mg content causes a rapid loss in relative ductility/quality and the samples fail short of the necking strain, which is in principle an expected result. However, the chart shows that a proportionally larger loss of relative ductility occurs at the higher Mg and Fe contents and that the deleterious effect is even larger at the larger DAS.

It is known that large π-$Al_8FeMg_3Si_6$ particles form when the Mg and Fe contents are above 0.5 and 0.04%, respectively.[12,13] These particles are detrimental to the alloy ductility and, because they tie up some of the Mg, also to the strength.[13,14] This accounts for the deleterious effect of increased Mg and Fe content. The detrimental effect of larger DAS on the ductility can also be related to the formation of π-phase particles, since these particles grow larger when the solidification rate is low.[14,15] A conclusion to be made from this simple analysis is that alloys with high Mg and Fe contents should be used in permanent mold applications to restrict the size of the π-phase particles.[9,11] Alternatively, the addition of an Fe-controlling element such as Be should be considered.[13,16]

These examples show that the analytical quality index chart is a very sensitive tool able to detect variations in the relative ductility. In this case, the loss of ductility is connected with changes in the microstructure that make the material more brittle without affecting the flow behavior (constant K value). A more detailed analysis of the quality index behavior of these alloys involving a wider range of data is presented elsewhere[8,9]

3.2 Case Study 2: K Constant, Q Variable

In Fig. 5, the true stress-true plastic strain flow curves[17] of samples of a sand-cast magnesium AZ91 alloy (Mg-9%Al-1%Zn) under different tempers are shown. The experimental curves are fitted to functions of the form of Eq 3. It is seen that a good fit is obtained with a single K value (570 MPa) by adjusting the n value according to the temper. Thus, in this regard, the Mg-base alloy can be expected to behave similarly to the Al-Si-Mg alloys A356 and A357 in the sense that a constant Q value

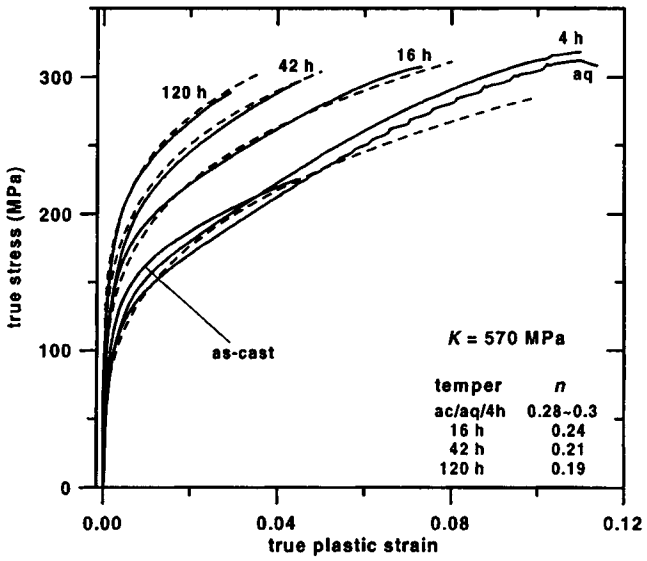

Fig. 5 True stress-true plastic strain flow curves of a magnesium alloy AZ91 aged for different times[17] at 165 °C. The dashed lines are functions of the form of Eq 3 fitted to the experimental curves, with given K and n values

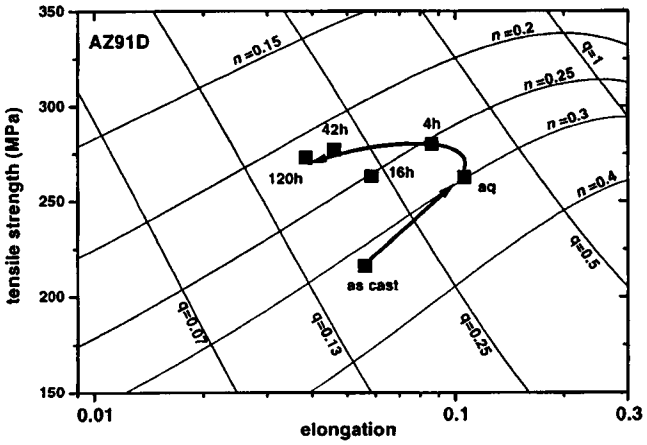

Fig. 6 A quality index chart for alloy AZ91 generated with Eq 4 and 6. K = 570 MPa and given n values. Experimental data from Ref 17

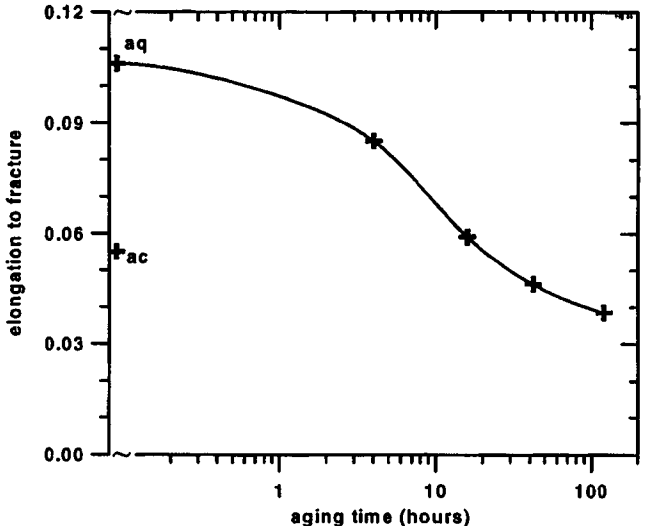

Fig. 7 The tensile elongation to fracture of an AZ91 alloy as a function of the aging time[17] (ac and aq stand for as-cast and as-quenched material, respectively)

should be observed as the aging time is increased. A quality index chart for alloy AZ91 generated with K = 570 MPa and a range of n values is shown in Fig. 6. The chart includes experimentally determined data showing the effect of the solution heat treatment and subsequent aging on the tensile strength and ductility of the material. Both the strength and ductility increase at short aging times, but, in contrast with aluminum alloys A356/357, at longer aging times, the strength remains constant while the ductility decreases. In terms of the relative ductility, the solution heat treatment increases the q value from about 0.15 for the as-cast samples to about 0.4 for the as-quenched samples, but then longer aging continuously lowers q down to about 0.15.

The reasons for this behavior are better explained in relation to Fig. 7, where a large monotonic drop in tensile ductility as the material is aged can be observed. The decrease in ductility is caused by the cellular precipitation of β-$Al_{12}Mg_{17}$ plates on the grain boundaries, which, in turn, causes a shift in the fracture mode from predominantly transgranular to predominantly intergranular.[18] The yield strength increases with aging time, as can be seen from the flow curves in Fig. 5, but the tensile strength remains virtually constant for the more aged samples (notice that the stress in Fig. 5 is the true stress while in Fig. 6 it is the engineering stress).

The chart in Fig. 6 shows that the relative ductility/quality of sand-cast alloy AZ91 is quite low, $q \cong 0.4$ at the best, and, potentially, the alloy could be up to 3 times more ductile as far the onset of necking is concerned (line with $q = 1$). Since the cracking of the discontinuously precipitated β-$Al_{12}Mg_{17}$ particles controls the ductility of the aged samples, a different aging temperature could modify the ratio of continuous to discontinuous precipitation, reducing the size of the large intergranular plates, and thus increase the ductility. Grain refining may subdivide the intergranular plates, possibly increasing the ductility as well.

As in the case of alloys A356/357, these examples show that the analytical charts help to identify changes in the microstructure that make the material relatively more brittle and provide a physically meaningful reference frame to assess the material's performance.

3.3 Case Study 3: Both K and Q Change

Two Sr-modified Al-4.5%Si-1%Cu-Mg alloys[5] with 0.1 and 0.5%Mg, respectively, are compared in this case. Selected flow curves of both alloys are plotted together in Fig. 8 (see Table 1 for the key to identify the heat treatment). The alloy with 0.5%Mg is significantly stronger but also less ductile. In general terms, as the materials are progressively aged toward peak aging, the yield strength increases while the ductility decreases. Overaging, on the other hand, lowers the yield stress but does not increase the ductility except for the more overaged samples. Samples with large DAS were also tested in the original study and found to be significantly less ductile than the samples with small DAS for all tempers.[5]

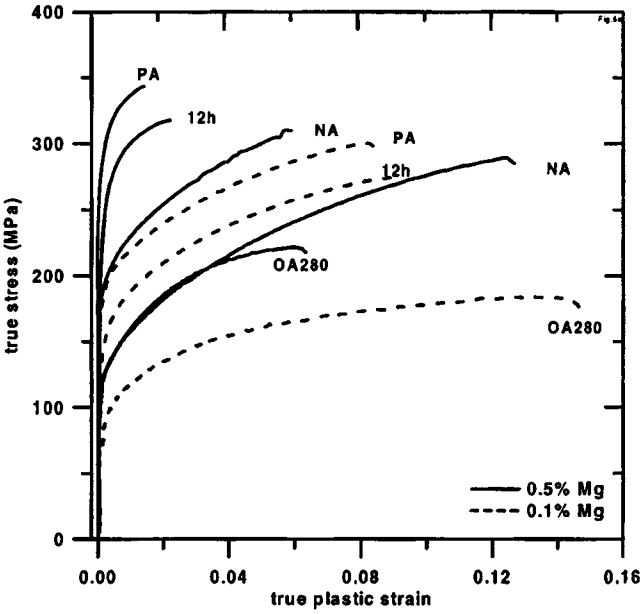

Fig. 8 Comparison of selected flow curves of two Al-Si-Cu-Mg alloys under different tempers (see Table 1 for the key to identify the samples). All samples with DAS = 25 μm

Table 1 Key to identify the heat treatments applied to the tensile samples of Fig. 8 and 9

DAS (μm)	Natural Aging (a)	12 h 160 °C	32 h 160 °C	20 h 220 °C	24 h 280 °C
25	NA	12 h	PA	OA220	OA280
50	NA50	. . .	PA50	. . .	. . .

(a) Natural aging: 3 to 8 weeks at room temperature.

The parameters of the flow curves of Fig. 8 have been condensed in Table 2. For both alloys, the underaged curves and up to peak aging could be fitted reasonably well with strength coefficients *K* of about 500 and 460 MPa for the alloy with 0.1 and 0.5%Mg, respectively. The *n* value decreased with aging for both alloys. The yield strength of the overaged samples decreased while a high strain hardening rate region developed at low strains followed by a low strain hardening rate stage at large strains. The *K* value decreased considerably in comparison with the underaged condition for both alloys, but especially for the 0.1%Mg alloy.

In Fig. 9, a quality index chart for the alloys has been created using the parameters of Table 2. For simplicity and in order to be able to compare both alloys on a common base, a single "average" *K* value (= 485 MPa) was assumed valid for the underaged and peak-aged conditions of both materials, for the range of *n* values indicated in the figure. The experimental data points are plotted in the figure as well, and it is seen that for both alloys the data describe an approximate circular path.

Figure 9 provides a concise description of the effect of aging time, Mg content, and DAS on the tensile behavior. In the alloy with 0.1% Mg, aging up to peak aging (compare samples NA and PA) keeps the relative ductility/quality constant. On the contrary, there is some loss of quality in the alloy with 0.5% Mg.

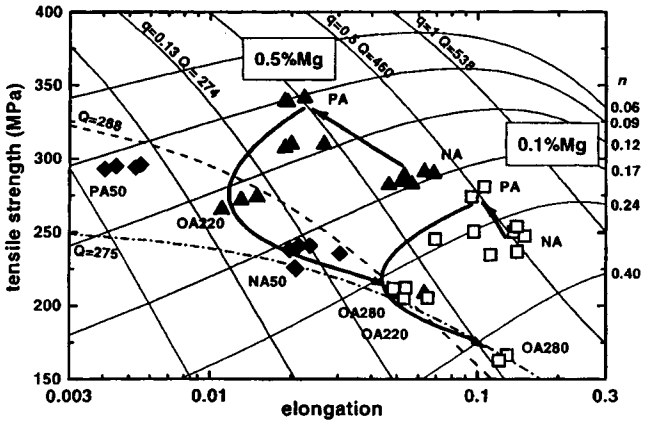

Fig. 9 A quality index chart and tensile data for the two Al-Si-Cu-Mg alloys.[5] The arrows indicate the strength-ductility path for samples with DAS = 25 μm

Table 2 The strength coefficient, K, and the strain hardening exponent, n, of the Al-Si-Cu-Mg alloys, as determined from the flow curves of Fig. 8 (see Table I for key to the heat treatment)

0.1% Mg alloy	*K* (MPa)	*n*	0.5% Mg alloy	*K* (MPa)	*n*
NA	500	0.26	NA	465	0.15
4 h	500	0.29	12 h	460	0.09
PA	485	0.18	PA	460	0.07
OA220	290	0.10	OA220	380	0.07
OA280	255	0.14	OA280	340	0.15

Overaging, on the other hand, causes a sharp fall of quality in both alloys as the data points follow a circular path.

For a given temper, a higher Mg content generally lowers the relative ductility/quality of the material. The effect is stronger in the peak-aged condition. Roughly speaking, the *q* values of the 0.5% Mg alloy are a factor of 2 lower than for the alloy with 0.1% Mg. Similar to alloys A356/357, this difference is related to the formation of π-phase particles in the alloy with higher Mg content.[19]

A large DAS has a strong detrimental effect on the alloy's relative ductility (compare samples NA and PA with NA50 and PA50, respectively, for the alloy with 0.5% Mg). This is due to the increased size of the π-phase particles as well as to a larger porosity content.[5] On the other hand, notice that the data points NA and NA50 and PA and PA50 are approximately on the same flow lines. This means that the DAS affects the ductility but not the strain hardening behavior.

The circular paths described by the experimental data points in Fig. 9 can be understood in terms of the variation in *K* value as the material is overaged (Table 2). Up to peak aging, the data points follow an ascending path (arrows between NA and PA data points). The *K* value is high and remains constant. By virtue of Eq 9, the *Q* value is high as well. As the alloys are overaged, *K* and hence *Q* decrease. The iso-*q* lines need to be recalculated according to the new *K* value (Eq 6). The recalculated iso-*q* lines are represented in Fig. 9 by the dashed (0.5% Mg) or dash-dot (0.1% Mg) lines, and it is seen that the data points of the overaged

materials tend to follow them. The net overall effect of a continuously decreasing K value is the observed circular path in the strength-ductility relationship. A similar behavior has been reported in an Al-Cu-Mg-Ag casting alloy.[3,20]

The differences in behavior between the Al-7Si-Mg and the Cu-containing alloys can be explained by differences in their precipitation hardening characteristics. In the Al-Mg-Si system, the hardening precipitates are small coherent β'' and semicoherent β'-Mg/Si, which produce a large increase in the yield strength. When the material is plastically deformed, these precipitates are easily cut by dislocations, even when the material is overaged.[21–23] No significant changes in the micromechanisms of deformation occur as aging progresses and Fig. 3 shows that overaging results in increased ductility as the material loses strength[10,20] such that both K and Q remain approximately constant.

In contrast, the structure of the precipitates and hence the deformation mode change dramatically in Al-Si-Cu-Mg alloys with aging. At moderate aging temperatures, hardening is due to the formation of Guinier-Preston zones,[24] which leads to high yield strength and decreasing strain hardening rate. Up to peak aging, the behavior is thus similar to the Al-Si-Mg system. Overaging, however, results in the simultaneous formation of relatively large θ' plates and small $S'Al_2CuMg$ needles,[25] which are hard nonshearable obstacles to dislocations. Nonshearable obstacles lead to lower yield strength and, at low strains, high strain hardening rate due to the accumulation of Orowan loops around the strengthening particles.[24] As the strain is increased, the build up of primary shear loops generates intense stress fields around the strengthening precipitates. These stresses are limited[26] by the activation of cross-slip and secondary dislocation processes, which thus reduce the strain hardening ability of the material. Bauschinger effect experiments[24] have shown that saturation of the internal stress occurs at strains of about 3.5 to 4% in Al-4% Cu-1.2% Mg alloys. Saturation of the internal stresses generated by the strengthening precipitates results in a low strain hardening rate, which, in turn, results in the decreased K value (and hence Q value) of the overaged materials at large strains.[3,5]

The main observations stemming from the application of the quality index charts to Al-Si-Cu-Mg alloys are the overall low relative ductility of the alloys, the detrimental effect of the π-phase particles on the alloy with 0.5% Mg, and, more importantly, the rationalization of the circular pattern of the strength-ductility relationship.

4. Boundary to Microstructural Improvement

The charts presented in Fig. 4, 6, and 9 illustrate the power of the analytical method to generate dedicated quality index charts for any material from the knowledge of only two material parameters, K and n. The iso-q lines represent contour lines of constant strain hardening[2] and are able to identify shifts in the ductility due to microstructural factors that will not affect the strain hardening mechanisms, *e.g.*, the presence of porosity or the formation of second-phase particles. If the material's strength coefficient K is affected by changes in the chemical composition or the tempering, the charts can be naturally modified and the material behavior accounted for as well.

A most significant feature of the charts is that they locate the maximum tensile ductility available to the material in terms of its strain hardening ability (line with $q = 1$) and thus provide a natural reference frame for the assessment of the alloy properties. This feature can be used to provide a unified view of different materials, as follows.

Equation 9 shows that the Q value can be considered as a sole function of K. This relationship incorporates into the model the fact that K may vary depending on the material and the temper. This is illustrated by Fig. 10, where the solid lines have been calculated using Eq 9, for a range of q values. The data points representing the different materials are Q values calculated using Eq 8 with K and n values according to the different materials and tempers. For a given K value, the range of data points represents the variation in q value, caused by the different DAS, inclusions and second-phase particle content, porosity, *etc.*, for the particular material/temper combination. For sound samples with small DAS, the ductility is at its highest and may approach the limit given by the onset of necking, *i.e.*, the line with $q = 1$ in Fig. 10. In other words, the region above the line $q = 1$ cannot be accessed in tensile deformation, which can thus be seen as an upper bound to the effect of microstructural improvement on the tensile properties. The Q-K chart of Fig. 10 can also be used to find combinations of chemical composition and temper that maximize the Q value of a particular alloy system, as explained in detail in Ref 8.

In terms of relative ductility, Fig. 10 shows that alloys A356/A357 perform the best. The Al-Si-Cu-Mg alloys tend to have low relative ductility, although the Q value is high for small DAS due to the alloy's high strength. The detrimental effect of the formation of π-phase particles on the alloy with 0.5% Mg is also clear from this plot. The Mg-based alloy, on the other hand, has a relatively high Q value, although its performance in terms of relative ductility is not very good.

5. Summary and Conclusions

An analytical method of generating quality index charts for any alloy system has been presented.

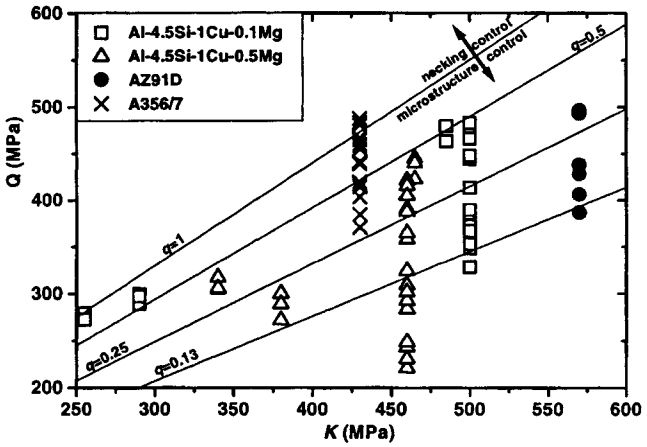

Fig. 10 The quality index as a function of the material strength coefficient, K, for the studied alloys. The solid lines have been calculated with Eq 9, and the individual data points with Eq 8.

The analytical charts provide an overview of the strength-ductility relationship of the material and allow for a systematic assessing of the effect of temper, microstructural parameters, and chemical composition on the mechanical performance of the material.

The lines of constant relative ductility help to identify shifts in the ductility due to microstructural factors that do not affect the strain hardening behavior of the material. Should the strain hardening behavior be affected during aging, this is reflected in the chart by changes in the location and slope of both flow curves and constant relative ductility lines.

The charts allow for comparisons with other alloy systems, using the necking onset strain as a reference, and locate the upper boundary to the maximum ductility of the material. For any given temper, the charts indicate the limits to the possible improvements in the microstructure.

Acknowledgments

The author is indebted to J. Barresi and M.J. Couper, Comalco Aluminum Ltd., for the unpublished data shown in Fig. 4. Support from the Australian Government's Cooperative Research Centres Program is gratefully acknowledged.

References

1. M. Drouzy, S. Jacob, and M. Richard: *AFS Int. Cast Met. J.*, 1980, vol. 5, pp. 43–50.
2. C.H. Cáceres: *Int. J. Cast Met. Res.*, 1998, vol. 10, pp. 293–99.
3. C.H. Cáceres, T. Din, A.K.M.B. Rashid, and J. Campbell: *Mater. Sci. Technol.*, 1999, vol. 15, pp. 711–16.
4. C.H. Cáceres: *AFS Trans.*, 1998, vol. 106, pp. 601–04.
5. C.H. Cáceres, J.H. Sokolowski, and P. Gallo: *Mater. Sci. Eng. A*, 1999, vol. 271, pp. 53–61.
6. C.H. Cáceres, L. Wang, D. Apelian, and M. Makhlouf: *AFS Trans.*, 1999, vol. 107.
7. G.E. Dieter: *Mechanical Metallurgy, 3rd ed.*, McGraw-Hill, New York, NY, 1986, pp. 290.
8. C.H. Cáceres: *Int. J. Cast Met. Res.*, Vol. 12, 2000, in press.
9. C.H. Cáceres and J. Barresi: *Int. J. Cast Met. Res.*, vol. 12, 2000, in press.
10. S. Shivkumar, C. Keller, and D. Apelian: *AFS Trans.*, 1990, vol. 98, pp. 905–10.
11. J. Barresi, M.J. Kerr, H. Wang, and M.J. Couper: *AFS Trans.*, vol. 108, 2000, in press.
12. B. Closset and J.E. Gruzleski: *Metall. Trans. A*, 1982, vol. 13A, pp. 945–51.
13. G.E. Nagel, J.P. Mouret, and J. Dubruelh: *AFS Trans.*, 1983, vol. 91, pp. 157–60.
14. C.H. Cáceres, C.J. Davidson, J.R. Griffiths, and Q.G. Wang: *Metall. Mater. Trans. A*, 1999, vol. 30A, pp. 2611–18.
15. Q.G. Wang, C.H. Cáceres, and J.R. Griffiths: *AFS Trans.*, 1998, vol. 106, pp. 131–36.
16. D.A. Granger, R.R. Sawtell, and M.M. Kersker: *AFS Trans.*, 1984, vol. 92, pp. 579–86.
17. C.L. Bancroft, C.H. Cáceres, and J.R. Griffiths: *Proc. Magnesium Technology 2000 Int. Conf., Nashville, TN, Mar. 2000.*
18. C.H. Cáceres, C.L. Bancroft, J.R. Griffiths, and C.J. Davidson: 2000, in preparation.
19. R. Smith, C.H. Cáceres, and D. StJohn: *Materials Research 96, IMMA Conf. Proc., Brisbane, July 1996*, The Institute of Metals and Materials Australasia, Brisbane, 1996, vol. 3, pp. 140–43.
20. T. Din, A.K.M.B. Rashid, and J. Campbell: *Mater. Sci. Technol.*, 1996, vol. 12, pp. 269–73.
21. J.M. Dowling and J.W. Martin: *Acta Metall.*, 1976, vol. 24, pp. 1147–53.
22. K. Banizs: *Mater. Sci. Eng. A*, 1979, vol. A41, pp. 17–24.
23. L. Zhen and S.B. Kang: *Metall. Mater. Trans. A*, 1997, vol. 28A, pp. 1489–97.
24. R.E. Stoltz and R.M. Pelloux: *Metall. Trans.*, 1976, vol. 7A, pp. 1295–1306.
25. W. Reif, J. Dutkiewicz, R. Ciach, S. Yu, and J. Krol: *Mater. Sci. Eng. A*, 1997, vol. A224–A236, pp. 165–68.
26. M.F. Ashby: in *Strengthening Methods in Crystals*, A. Kelly and R.B. Nicholson, eds., Elsevier, Amsterdam, 1971, ch. 3.